# Idealized digital models for conical reed instruments, with focus on the internal pressure waveform

Jean Kergomard, Philippe Guillemain, Fabrice Silva, Sami Karkar

# Idealized digital models for conical reed instruments, with focus on the internal pressure waveform

J. Kergomard[*], P. Guillemain, F. Silva

LMA, CNRS, UPR 7051, Aix-Marseille University, Centrale Marseille,
F-13453 Marseille Cedex 13, France

S. Karkar

LEMA, EPFL, Station 11 Route cantonale, CH-1015 Lausanne, Suisse.

January 14, 2016

## Abstract

Two models for the generation of self-oscillations of reed conical woodwinds are presented. They use the fewest parameters (of either the resonator or the exciter), whose influence can be quickly explored. The formulation extends iterated maps obtained for lossless cylindrical pipes without reed dynamics. It uses spherical wave variables in idealized resonators, with one parameter more than for cylinders: the missing length of the cone. The mouthpiece volume equals that of the missing part of the cone, and is implemented as either a cylindrical pipe (first model) or a lumped element (second model). Only the first model adds a length parameter for the mouthpiece and leads to the solving of an implicit equation. For the second model, any shape of nonlinear characteristic can be directly considered. The complex characteristics impedance for spherical waves requires sampling times smaller than a round trip in the resonator. The convergence of the two models is shown when the length of the cylindrical mouthpiece tends to zero. The waveform is in semi-quantitative agreement with experiment. It is concluded that the oscillations of the positive episode of the mouthpiece pressure are related to the length of the missing part, not to the reed dynamics.

PACS: 43.75 Ef, 4375 Pq
Keywords: musical instruments, reed instruments, bassoon, oboe, saxophone

## I. INTRODUCTION

Simplified models with a minimal number of parameters are helpful tools for the understanding of the physical principles of the musical instruments. A famous example was given by the paper by Mc Intyre et al[1]. In particular, they proposed in Appendix A of their paper the relation between the functioning of simplified clarinet-like instruments (a cylinder without holes) and the iterated map theory. The corresponding model is based upon the assumption of the absence of both losses and reed dynamics. Only three parameters are needed: two parameters of the excitation (the mouth pressure and a composite reed parameter) that can be deduced from a static, nonlinear characteristic of the reed-mouthpiece system, and one for the resonator (the length). Thus the radius does not appear explicitly in the model and can be chosen arbitrarily (in the limit of the one-dimensional theory). Concerning the waveform of the acoustic pressure inside the mouthpiece for periodic regimes, this model yields a caricature in the form of square signals, therefore with missing even harmonics. However the model makes possible deducing several properties, such as the duration of the transient and the nature, amplitude and stability of possible regimes. This was done in several papers, based upon the nonlinear characteristic proposed in Ref. [2], and with a supplementary parameter, corresponding to frequency-independent losses in the resonator.[3,4,5] Comparison with experiments shows a good agreement for the bifurcation scheme.[6] Therefore, thanks to these extremely simplified models, basic features of the sound production can be understood, while refined details of the waveform, that are important for the high frequencies and the external sound perception, cannot be predicted.

The purpose is here to extend this kind of model to simplified conical reed instruments, like bassoon, oboe or saxophone, i.e., to diverging truncated cones, without holes and but with a mouthpiece in order to understand the influence of the main parameters on the waveform, not to provide useful synthesis schemes or detailed spectral analysis as in Ref. [7]. In Ref. [8], it was shown that the pressure waveform in the mouthpiece of a saxophone is rather similar to that of a stepped cone or that of a "cylindrical saxophone".[10] Such an instrument is a cylindrical tube excited by a reed at the respective distances $x_1$ and $\ell$ of the two extremities. By analogy with the bowed string, the excitation point is defined by the ratio $\beta = x_1/(x_1 + \ell)$. For these instruments the idealized waveform of the steady-state regime in the mouthpiece was shown to be a rectangle signal, equivalent to the pure Helmholtz motion

[*]Tel: (+33)4 8452 4224,
Email: kergomard@lma.cnrs-mrs.fr

for bowed-string instruments, and the extension of the iterated map method is straightforward. For reed instruments, the Helmholtz motion is defined by a succession of two episodes of constant mouthpiece pressure.[8] The ratio of the negative pressure time to the oscillation period is equal to $\beta$, while the pressure values are $-p_m(1-\beta)/\beta$ and $p_m$, respectively, where $p_m$ is the mouth pressure.
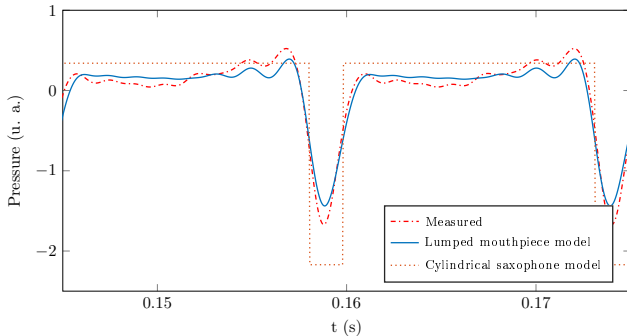


Figure 1: (Color online) Comparison of the measured mouthpiece pressure for a baritone saxophone on the lowest note C2 (65.4Hz, dash-dotted line) with the signal obtained using the second model presented in the current paper (using $\ell = 2.272m$, $x_1 = 30.8cm$, $\gamma = 0.34$ and $\zeta = 0.51$, notations defined in Sec. IV, solid line) and with the rectangle signal obtained using the "cylindrical saxophone" model (same values of $\ell$, $x_1$ and $\gamma$, see Ref. 10, dotted line). The numerical result is discussed in Section V.D. Measurement done by B. Gazengel.

However the measurement of a mouthpiece pressure signal of a saxophone shows significant differences from a rectangular signal, in particular the negative pressure episode has the shape of a triangle (see Fig. 1), and there is an increasing oscillation during the positive pressure episode. The reason probably lies in the validity limit of the analogy, which supposes that the missing cone is short compared to the wavelength. Interest in the measured waveforms is rather rare in the literature, but similar shapes were found by several authors for this kind of instruments.[8,11,12,13]

Therefore the question addressed in this paper is the following: is it possible to find a waveform similar to the measured ones with a model generalizing the iterated map model to conical instruments, i.e., ignoring both losses and reed dynamics? Fig. 1 shows an attempt of comparison of a measured mouthpiece pressure with the model studied in the present paper, and with the corresponding pure Helmholtz motion (the method used for this figure is detailed and discussed in Section V).

Compared with a cylinder, at least one supplementary parameter is needed for such a model, e.g., the length of the missing cone. It will be shown that this is sufficient to introduce a great complexity. Notably, the reed dynamics is not needed to reproduce the oscillation increase during the positive pressure episode. We also remark that in order to provide the simplest

models, it is not sufficient to change the values of the parameters in more complete existing digital schemes. As examples, the suppression of losses can make some schemes instable, and the scheme proposed in Ref. 14 accounts for a reed dynamics with a possibly huge but still finite reed natural frequency.

The paper focuses on the waveform of regimes similar to that shown in Fig. 1. Other types of regimes can be found, such as octave regime, inverted Helmholtz motion,[8] or quasi-periodic regimes,[15] but are not investigated here.

In Section II, the classical model of reed instruments, based upon that of Wilson and Beavers,[2] is summarized. Sec. III discusses the general methods of computation of self-oscillations based upon either the impulse response or the reflection function of the resonator for an instrument with arbitrary shape. Then (Sec. IV) a digital model for a truncated cone with a cylindrical mouthpiece is given: it takes advantage of the spherical wave decomposition and is built upon three geometrical parameters. Furthermore, keeping the idea of setting the mouthpiece volume, a second model, which does not require any parameter for the mouthpiece, is presented in Section V. A conclusion is given in Section VI. Appendix A provides further details on the stability of the impedances of the digital implementations.

The idea of these two models was already published in Ref. 16, but the continuous and discrete-time equations were not written. No comparison of the convergence of the two models was given, because the main focus of this reference was on the difference between wide and narrow reed opening, i.e., on the difference between a double and a single reed mouthpiece.

## II. CLASSICAL MODEL FOR REED INSTRUMENTS AND NONLINEAR QUASI-STATIC CHARACTERISTIC

The simplified model used in this paper ignores the reed dynamics (i.e. the inertia and damping of the reed): when the reed does not beat, the reed displacement is proportional to the pressure difference across the reed. Moreover the flow produced by the reed movement is ignored. The model is based upon two acoustic unknowns at the input of the resonator, the flow rate $u(t)$ and the pressure $p(t)$, and two equations: the first one is the resonator input impedance relationship (which is linear), and the second is a nonlinear time-domain relationship:

$$u(t) = Y_c F[p(t)], \tag{1}$$

assumed to be quasistatic. $Y_c = S_{in}/(\rho c)$ is the characteristic acoustic admittance of a cylindrical resonator having the cross section $S_{in}$ ($\rho$ is the density of air, $c$ is the velocity of sound).

In the quasistatic regime, the acoustic velocity in the reed channel is approximated by means of the steady Bernoulli equation[2,17]. It is proportional to $\text{sign}(\Delta p)\sqrt{|\Delta p|}$, where $\Delta p = p_m - p$ is the pressure difference across the reed. $p$ denotes the pressure at

the output of the reed channel, equal to that at the resonator input; $p_m$ is the pressure inside the mouth of the player. Furthermore it is assumed that the cross section area of the reed channel aperture depends linearly on the reed displacement. Therefore, when the reed dynamics is ignored, it is proportional to the pressure difference. When the pressure difference reaches the closure pressure $p_M$, the channel closes and the flow is blocked. Therefore if $\Delta p \le p_M$ the flow rate $u$ is proportional to $\mathrm{sign}\,(\Delta p)\sqrt{|\Delta p|}$, while if $\Delta p > p_M$, the flow vanishes. Two dimensionless parameters $\gamma$ and $\zeta$ are defined:

$$\gamma = \frac{p_m}{p_M} \text{ and } \zeta = \frac{cS_{op}}{S_{in}}\sqrt{\frac{2\rho}{p_M}}. \qquad (2)$$

$S_{op}$ is the cross-section area of the reed channel opening at rest. $\zeta$ is inversely proportional to the square root of the reed stiffness, contained in $p_M$. In real single-reed instruments, typical values of the parameters are $\gamma \in [0, 1.5]$ and $\zeta \in [0.1, 1]$, while for double reeds it can exceed 2 (see Ref. 11). The function $F(p)$ is piecewise analytic with a singular point at $p = p_m$ ($\Delta p = 0$), and not derivable at $p = p_m - p_M$ ($\Delta p = p_M$). Fig. 2 shows the function $F(p)$. Notice that experiments showed that for double reed instruments, this function is not very different.[18] Eventually the function $F(p)$ is defined by:

$$F(p) = \zeta p_M \left[1 - \gamma + \frac{p}{p_M}\right]^+ \mathrm{sign}\left(\gamma - \frac{p}{p_M}\right)\sqrt{\left|\gamma - \frac{p}{p_M}\right|} \qquad (3)$$

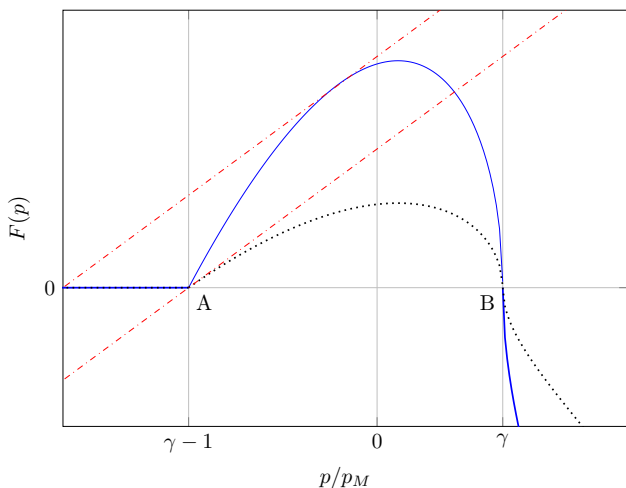with the positive part $[x]^+ = x$ if $x \ge 0$, 0 otherwise.



Figure 2: (Color online) Nonlinear characteristic $F(p)$. Solid line: $\zeta = 2.55$. Dotted line: $\zeta = 0.95$. The point A indicates the beating limit; the point B indicates the limit of negative flow rate. Between the dash-dotted lines, Eq. (8) has 3 solutions when $\zeta > 1$ (see Sec. III).

## III. TWO GENERAL METHODS OF COMPUTATION FOR RESONATORS OF ARBITRARY SHAPE.

The present section states the problem of the computation of the response of resonators of arbitrary shape, and enhances the major concerns: solvability and computation cost expressed in terms of the time sampling and of the duration of the history to consider.

### A. The impulse response method

For a 1D, linear resonator, a general model is based upon Eq. (1) and:

$$p(t) = (h * u)(t) = \int_0^t h(t - t')u(t')dt'. \qquad (4)$$

The impulse response $h(t)$, inverse Fourier transform of the input impedance $Z(\omega)$, characterizes the resonator, which is assumed to be linear. Both $h(t)$ and $u(t)$ are causal, therefore the integral is limited to the interval $[0, t]$. As in Ref. 1, the time range on which the knowledge of the flow rate $u$ is needed in order to compute $p(t)$ defines the *duration of the history*. The first method of computation of $u(t)$ given $p(t)$ is the direct solving at each time $t$ of Eqs. (1) and (4), the former being instantaneous.

Then, for given initial conditions, the *solvability* requires that the evaluation of Eq. (4) should not rely on the knowledge of the flow at the current instant $t$. This can be achieved numerically by subdividing the integration range with time step $t_s$, and approaching the integrand by a piecewise constant function whose value is $h(t - t_n)u(t_n)$ for $t \in [t_n, t_{n+1})$. This is known as the left rectangle rule, such as

$$p(t_n) = t_s \sum_{m=0}^{n-1} h(t_n - t_m)u(t_m) \text{ with } t_m = mt_s. \qquad (5)$$

Though more accurate than the left rectangle rule, the trapezoidal rule may not be suitable, as the pressure $p(t_n)$ could not be deduced explicitly from the history of the flow $u(t_m < t_n)$. Solving Eqs. (1) and (5) is direct, without any inversion. Another concern is the fact that the impulse response $h$ should be well approached by its sampled version $h(t_n)$. The *time sampling*, i.e., the time step $t_s$, has to be adapted to the smoothness of the impulse response $h(t)$.

Finally the main drawback (see Ref. 1) is that the history of $h$ is in general unbounded, resulting in a numerically expensive integration. In order to reduce the duration of the history, Mc Intyre et al[1] suggested to slightly modify these equations, by using the d'Alembert decomposition into traveling waves, as explained hereafter.

### B. The reflection function method

If a portion of cylindrical tube is considered at the input of the instrument, two new unknowns are the

incoming and outgoing plane waves ($p^-(t)$ and $p^+(t)$, respectively) at the input of the tube:

$$p = p^+ + p^-; \quad Z_c u = p^+ - p^- \qquad (6)$$

($Z_c = Y_c^{-1}$). Using those, Eq. (4) is replaced by:

$$p^-(t) = \left(r * p^+\right)(t) = \int_0^t r(t-t')p^+(t')dt', \qquad (7)$$

where $r(t)$ is the reflection function (of planar waves). Two advantages can be found. First, as soon as a cylindrical portion of finite length exists at the input of a resonator of any shape, it introduces some delay in the traveling waves so that $r(0) = 0$ and the incoming wave is 0 at time $t = 0$. The problem then consists of solving at each time simultaneously Eq (1) and

$$Z_c u(t) = p(t) + p_h(t), \qquad (8)$$

with $p_h(t) = -2p^-(t) = -2\left(r * p^+\right)(t)$ usually referred to as the "history" of the acoustic pressure. This can be solved using a graphical method[19] as the intersection in the $(p(t), u(t))$-plane between the nonlinear function $u = Y_c F(p)$ and the straight line defined by Eq. (8). Equivalently, rotating the $(p(t), u(t))$-plane into the $(p^-(t), p^+(t))$-plane, it is possible to look at the intersection of another straight line defined by Eq. (7) and a function $G$, obtained by a change in variables from the function $F$[20]:

$$p^+(t) = G\left(-p^-(t)\right). \qquad (9)$$

For the particular case of Eq. (3), the analytical expression of Eq. (9) is given in Appendix A of Ref. 4. For $\zeta > 1$, three solutions can exist for Eq. (9), and a selection method needs to be defined, based upon the continuity of the function $p^-(t)$.[16]

The second advantage is that the history of $r(t)$ is in general much shorter than that of $h(t)$. For a purely cylindrical instrument of length $\ell$, without losses and with zero radiation impedance, the reflection function is a single delta function, $r(t) = -\delta(t - 2\ell/c)$, and the coarsest sampling time is a half round trip, $\ell/c$, at least when the initial condition can be discretized with the same time step, for example for the case of the excitation pressure $\gamma$ being a simple step or a piecewise constant function.

More generally, for any resonator having a cylindrical section with length $y$ at its entrance, accounting for the propagation delay $y/c$ of the traveling waves $p^\pm$ in the cylindrical section, Eq. (7) can be replaced by the following:

$$p^-(t) = \int_0^{t-2y/c} r_y(t')p^+(t-2y/c-t')dt', \qquad (10)$$

where $r_y$ is the reflection function at the output of the cylindrical part of the resonator. The upper limit of the integral is $t-2y/c$ because $p^+(t)$ is a causal signal. This allows computing the integral with the trapezoidal rule, ensuring a slightly smaller error that the left rectangle rule.

## IV. TRUNCATED CONE WITH A CYLINDRICAL MOUTHPIECE (FIRST MODEL)

The abovementioned methods can be used for truncated cones, in particular the method using the plane reflection function. However Refs. 24 and 25 show that this function is of infinite extent, and this would require the knowledge of the *ab initio* history to compute $p^-(t)$ in Eq. (7). Therefore the present paper considers the spherical reflection function as did Ref. 26.

For cylindrical instruments, simplified models can include the mouthpiece in the resonator. For conical instruments, this is not possible, and in general a truncated cone without mouthpiece can hardly produce periodic sounds. As it is known since Benade,[21] the harmonicity of the truncated cone can be improved by choosing a mouthpiece volume roughly equal to that of the missing cone. Thus, if this volume is set by means of a cylindrical mouthpiece, a new parameter is introduced (either the length $y$ of the mouthpiece or its cross section area $S_m$) and this leads to the first model, described in the present section. The matching of the plane waves in the cylindrical mouthpiece with the spherical waves in the cone can be done with an excellent precision,[22] but for the present purpose, the continuity of the flow rate and mean pressure is assumed between the output of the cylinder and the input of the cone. Fig. 3 shows the main geometrical parameters as well as an equivalent electrical circuit of the model described hereafter.
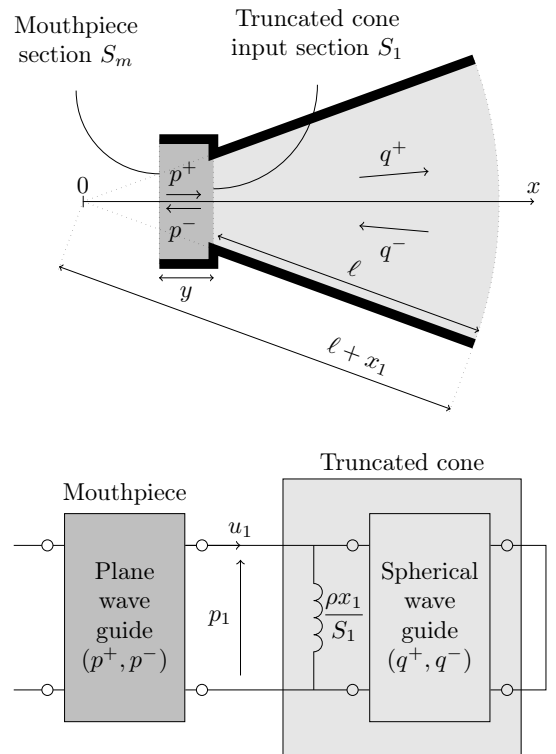


Figure 3: Geometry and equivalent circuit of the model with a cylindrical mouthpiece. The geometry of the truncated cone is described by 2 parameters only: $x_1$ and $\ell$.

## A. Equation at the input of the truncated cone

In the frequency domain (with $k = \omega/c$ the wavenumber), the solution of the Helmholtz equation in the conical tube with cross-section area $S(x)$ can be written as:

$$
\begin{align}
P_{\text{cone}}(x) &= Q^+(x) + Q^-(x); \tag{11}\\
U_{\text{cone}}(x) &= \frac{S(x)}{\rho c}\left(Q^+(x) - Q^-(x) + \frac{P_{\text{cone}}(x)}{jkx}\right)
\end{align}
$$

for $x_1 \leq x \leq x_1 + \ell$, where $x_1$ is the length of missing cone. $Q^\pm = a^\pm \exp(\mp jkx)/x$ are the incoming and outgoing spherical pressure waves, corresponding to the decomposition in traveling waves. For the remainder of the paper, capital letters discriminate frequency-domain quantities ($P_{\text{cone}}$, $U_{\text{cone}}$, $Q^+$ and $Q^-$) from their time domain counterparts ($p_{\text{cone}}$, $u_{\text{cone}}$, $q^+$ and $q^-$), and quantities indexed by 1 refer to values at the input of the truncated cone ($x = x_1$): $S_1 = S(x_1)$, $Q_1^+ = Q^+(x_1)$, $Q_1^- = Q^-(x_1)$, $P_1 = P_{\text{cone}}(x_1)$ and $U_1 = U_{\text{cone}}(x_1)$. In addition $P_1^+$ and $P_1^-$ are defined by

$$
\begin{align}
P_1^+ &= (P_1 + \rho c U_1/S_1)/2; \tag{12}\\
P_1^- &= (P_1 - \rho c U_1/S_1)/2; \tag{13}
\end{align}
$$

or, equivalently,

$$
P_1 = P_1^+ + P_1^- \text{ and } \frac{\rho c}{S_1}U_1 = P_1^+ - P_1^-. \tag{14}
$$

This resembles to a decomposition in planar, traveling waves of the input pressure and flow (see Eq. (6)), but is nothing more than the change in variables. Combining Eq. (11) at $x = x_1$ and Eq. (14) and eliminating $U_1$ lead to:

$$
\begin{align}
P_1^+ + P_1^- &= Q_1^+ + Q_1^-; \tag{15}\\
P_1^+ - P_1^- &= Q_1^+ - Q_1^- + \frac{P_1}{jkx_1}, \tag{16}
\end{align}
$$

and then

$$
\begin{align}
Q_1^- - P_1^- &= \frac{P_1}{2jkx_1}; \tag{17}\\
Q_1^+ - P_1^+ &= -\frac{P_1}{2jkx_1}. \tag{18}
\end{align}
$$

In the time domain, these expressions write down to

$$
\begin{align}
p_1^-(t) &= q_1^-(t) - \frac{c}{2x_1}\int_0^t p_1(t')dt'; \tag{19}\\
q_1^+(t) &= p_1^+(t) - \frac{c}{2x_1}\int_0^t p_1(t')dt'. \tag{20}
\end{align}
$$

Assuming a lossless propagation in the cone and a perfect reflection at its open end leads to:

$$
q_1^-(t) = -q_1^+(t - \tau), \tag{21}
$$

where $\tau = 2\ell/c$. It is possible to include a frequency-independent radiation length correction. However, the purpose of the paper is to ignore losses, so that a zero radiation impedance is considered here. Finally the following expression replaces Eq. (7):

$$
p_1^-(t) = -p_1^+(t - \tau) - \frac{1}{2}\frac{c}{x_1}\int_{t-\tau}^t p_1(t')dt'. \tag{22}
$$

This equation relates to the one given in Ref. 23 without introducing any cylindrical sections. Its major interest lies in the finite duration of the integral, limited to a round trip in the resonator.

## B. Modeling the mouthpiece as a cylindrical pipe

The mouthpiece volume $V_m$ is chosen equal to that of the missing part of the truncated cone, i.e., $V_m = x_1 S_1/3$ (this choice is not discussed in this paper, see, e.g., Ref. 27). The length $y$ of the mouthpiece (or the cross section area $S_m = V_m/y$) is a supplementary parameter that controls the cross-section area ratio:

$$
\mu = S_m/S_1 = x_1/(3y). \tag{23}
$$

By enabling any positive value of $y$ and allowing a cross-section discontinuity, this model generalizes the "cyclone" model defined by Refs. 28 and 29. The incoming and outgoing plane waves at the input of the mouthpiece, $p^\pm(t)$, relate to the pressure $p_1$ and the flow $u_1$ at the input of the truncated cone accounting for the propagation delay $y/c$ in the cylinder and for the assumed continuity of flow rate and pressure at the change in cross section. The continuity equations can be expressed using the variables $p_1^\pm$ (see Eq. 14):

$$
\begin{align}
2p_1^+(t) &= (1+\mu)p^+(t - y/c) + (1-\mu)p^-(t + y/c);\\
2p_1^-(t) &= (1-\mu)p^+(t - y/c) + (1+\mu)p^-(t + y/c). \tag{24}
\end{align}
$$

Replacing $p_1^\pm$ and their sum $p_1$ by these expressions in Eq. (22) and shifting time by $y/c$ lead to the formulation of $p^-(t)$ as a function of the history only:

$$
p^-(t) = D(t) - \frac{1}{x_1(1+\mu)}I(t), \tag{25}
$$

where, defining $K = (\mu - 1)/(\mu + 1)$,

$$
\begin{align}
D(t) &= K\left(p^-(t - \tau) + p^+(t - 2y/c)\right) - p^+(t - \tau - 2y/c).\\
I(t) &= c\int_{t-\tau}^t p^+(t' - 2y/c) + p^-(t')dt'; \tag{26}
\end{align}
$$

These equations enable the evaluation of the incoming plane wave using only quantities defined at the input of the mouthpiece.

## C. Discretization

For the algorithm, the following symbols are used: $x_s$ and $t_s$ are the sampling length and time, respectively, related by $x_s = ct_s$ and:

$$
\tau = \frac{2\ell}{c}; \ \ell = Mx_s \text{ and } y = Nx_s. \tag{27}
$$

5

Taking advantage of the existence of the cylinder at the input of the truncated cone, the outgoing pressure $p^+$ appears only in past terms in $D(t)$. Conversely, the integral $I(t)$ has $t$ as an upper bound and involves $p^-(t)$. It is approached using the trapezoidal rule:

$$
\begin{aligned}
I(t = nt_s) \simeq & \frac{x_s}{2}(p_n^- + p_{n-2N}^+) \\
& + x_s \sum_{m=1}^{2M-1} (p_{n-m}^- + p_{n-m-2N}^+) \\
& + \frac{x_s}{2}(p_{n-2M}^- + p_{n-2M-2N}^+) \\
= & J_n + \frac{x_s}{2}p_n^-
\end{aligned}
\tag{28}
$$

defining $J_n$ after isolation of $p_n^-$. $J_n$ is equivalently defined from the following recursive equation

$$
\begin{aligned}
J_n = & J_{n-1} + \frac{x_s}{2}\left(2p_{n-1}^- + p_{n-1-2N}^+ + p_{n-2N}^+\right) \\
& - \frac{x_s}{2}\left(p_{n-2M}^- + p_{n-1-2M}^-\right. \\
& \left. + p_{n-2M-2N}^+ + p_{n-1-2M-2N}^+\right).
\end{aligned}
\tag{29}
$$

The discretization of Eq. (25) is then written as:

$$
p_n^- = D_n - \frac{1}{x_1(1+\mu)}\left(J_n + \frac{x_s}{2}p_n^-\right)
$$
$$
\text{with } D_n = K\left(p_{n-2M}^- + p_{n-2N}^+\right) - p_{n-2M-2N}^+ + .
\tag{30}
$$

Finally, the solution of Eq. (30) is simply:

$$
p_n^- = \left(D_n - \frac{J_n}{x_1(1+\mu)}\right)\left(1 + \frac{x_s}{2x_1(1+\mu)}\right)^{-1}.
\tag{31}
$$

At each time step, the following quantities are computed successively: $D_n$, $J_n$ and $p_n^-$. When coupling them with the excitation, the computation of $p_n^+$ relies on the modified function $G$ (Eq. (9)), i.e., the nonlinear characteristic adapted to wave variables $p^\pm$. The dimensionless parameter $\zeta$ in Eq. (2) is defined with $S_{in}$ equal to the input cross-section area $S_1$ of the truncated cone, disregarding the cross-section area $S_m$ of the mouthpiece that will vary in the simulations presented hereafter while a fixed value of $\zeta$ is maintained.

As already mentioned in Sec. III, for $\zeta > 1$, $G$ is multi-valued. A suitable choice is detailed in Ref. 16: it imposes to discard discontinuities of $p^+(t)$ when several solutions of Eq. 9 are possible. Gokhstein[11] observed that this difficulty appears for double reed instruments. This is one reason of the choice of a second model, which also avoids the addition of one parameter for the mouthpiece (see Sec. V).

**D. Numerical results**

For the simulation, the chosen initial condition is the following: the mouthpiece pressure is zero for negative times, then its value jumps to a fixed constant $\gamma$. Therefore for $t < 0$, $p_1 = Z_c u_1 = p_1^+ = p_1^- = 0$, and $p_1^-(0) = 0$; then $p_1^+(0) = p_1(0) = Z_c u_1(0) = G(0)$. The sampling length is $x_s = 1mm$ (this is the shortest possible length for the mouthpiece) so that the sampling frequency, $f_s = c/x_s$, is $340kHz$.
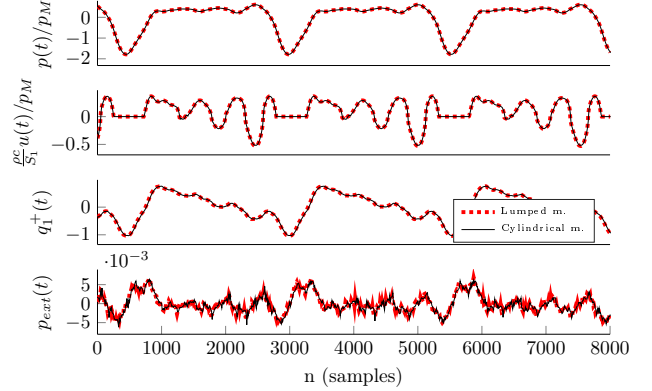


Figure 4: (Color online) Steady-state signals, for a very short length $y = 1mm$. From top to bottom: the dimensionless mouthpiece pressure $p(t)/p_M$; the flow rate at the input of the mouthpiece $u(t)$ times $\rho c/(S_1 p_M)$; the outgoing spherical wave $q_1^+(t)$ (arbitrary scale); the external pressure $p_{ext}(t)$ (arbitrary scale). The geometrical parameters are similar to those of a baritone saxophone ($\ell = 1m$, $x_1 = 0.3m$), the non dimensional mouth pressure and reed opening parameters are $\gamma = 0.4$, $\zeta = 0.95$, and the sampling length is $x_s = 1mm$. The dashed lines represent the result of the second model (see Section V).

Figure 4 shows four quantities of interest: the mouthpiece pressure $p(t)/p_M$; the flow rate at the input of the mouthpiece $u(t)\rho c/(S_1 p_M)$; the outgoing spherical wave $q_1^+(t)$; and the external pressure $p_{ext}(t)$ (discussed in Sec. IV.E). Some observations can be made: first, the V-shaped negative pressure episode is related to the vanishing of the flow, i.e., the beating of the reed on the lay. It is important to highlight that the V-shape of the negative pressure episode is induced neither by losses in the acoustic resonator, nor by a progressive beating of the reed (due to, e.g., the curvature of the mouthpiece lay) that is not included in the model of Eq. (3). A preliminary study shows that the oscillations during the positive pressure episode are essentially related to the length of the missing cone, $x_1$. The same applies to the duration of the beating of the reed. Finally, the flow rate becomes negative during a non negligible fraction of the period, contrary to the behavior of a cylindrical reed instrument.[4]

Fig. 5 shows how the result depends on the length $y$ of the mouthpiece (for a given volume). When $y$ tends to 0, the waveform converges to that obtained for the second model (described in Sec. V). This is enhanced in Fig. 6 in terms of spectral characteristics of the simulated pressure signals: the fundamental frequency and the magnitudes of the first coefficients of the Fourier series of the steady parts show the asymptotic behavior when increasing the mouthpiece cross section (i.e., decreasing its length $y$). For high values of $y$, the spec-
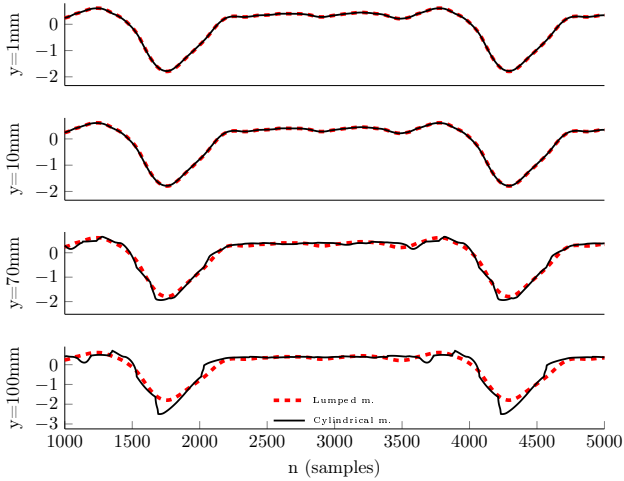
Figure 5: (Color online) Steady-state mouthpiece pressure $p(t)$ for various mouthpiece lengths $y$ (the parameter values are the same as those of Fig. 4). In abscissa, the number of samples. From top to bottom, the solid lines represent: $y = 1mm$ ($N = 1$, $\mu = 100$); $y = 10mm$ ($N = 10$, $\mu = 10$); $y = 70mm$ ($N = 70$, $\mu = 1.43$, value close to that of a real baritone saxophone); and $y = 100mm$ ($N = 100$, $\mu = 1$). For all plots the dashed line is the same: it represents the result of the second model.

tral characteristics do not exhibit monotonic behaviors. This may be related to the fluctuation that appears in the inharmonicity of the resulting resonators for $y$ increasing above the value of $50mm$ ($\mu$ below 2), as shown in Fig. 7. Fig. 5 also shows that when the length $y$ increases towards the case $\mu = 1$ used in Ref. 29, the waveform becomes less smooth. The smoothest waveform seems to correspond to short lengths, which is confirmed on Fig. 6 with the amplitude increase of the harmonics for $y > 60mm$ ($N > 60$). Here a mouthpiece is "short" when its cross-section is wide compared to that of the cone input. In comparison with values from Ref. 31, the inharmonicity of the present resonator remains, for $\mu > 1$, below the thresholds of quasi-periodic regimes. This does not hold for thin and long mouthpieces (i.e., $\mu < .5 \Leftrightarrow y > 200mm$): they do not always produce sound of the first register as do the larger and shorter mouthpieces.
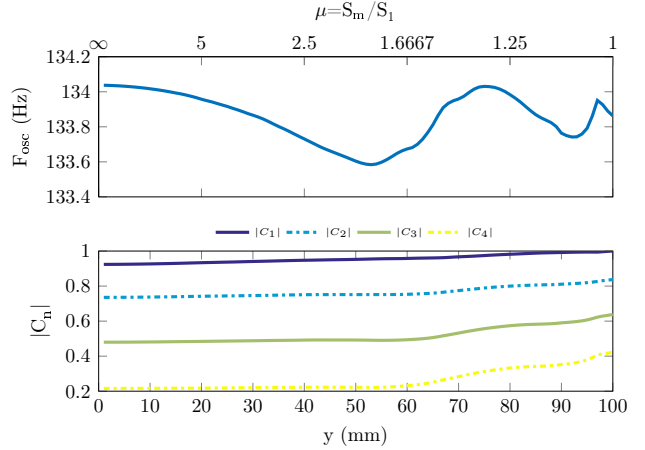


Figure 6: (Color online) Fundamental frequency (upper axes) and magnitude of the Fourier coefficients (lower axes) of the steady-state pressure signal as functions of the mouthpiece length $y$. The corresponding cross-section ratios values $\mu$ are also reported on the top of the upper axes. $C_1$ relates to the fundamental tone and $C_{n \geq 2}$ to the higher harmonics. All the other parameters values are the same as in Fig. 4.
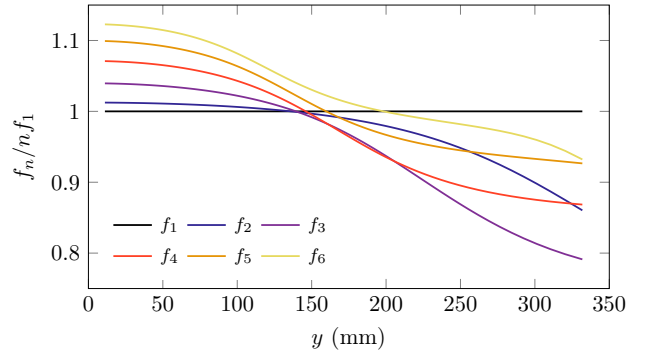


Figure 7: (Color online) Inharmonicity relative to the first resonance frequency of the first model, with respect to the mouthpiece length $y$ (all other parameters values are the same as Fig. 4).

### E. Radiated sound

For a cylinder, the use of a monopole model for the radiation at the open end transforms a square signal in its derivative, i.e., in an alternate Dirac comb. This simplified shape is confirmed by experiment.[30] Therefore it is interesting to use the same model for conical tubes, even if their radius is in general wider. If the monopole has a source-strength amplitude given by the output flow rate $U_{cone}(x_1 + \ell)$, the far-field radiated pressure can be approached with the following formula:

$$P_{ext}(\omega, r) = j\omega\rho U_{cone}(x_1 + \ell)\frac{e^{-jkr}}{4\pi r} \qquad (32)$$

where $r$ the distance to the monopole. More sophisticated models are possible, see for example Ref. 32 accounting for the spherical wavefronts. Because the pressure at the cone outlet $P_{cone}(x_1 + \ell)$ is assumed to

be zero, Eq. (11) leads to the simple result:

$$U_{\text{cone}}(x_1 + \ell) = 2\frac{S_2}{\rho c}Q^+(x_1 + \ell) \propto e^{-jk\ell}Q_1^+, \quad (33)$$

where $S_2 = S(x_1 + \ell)$ is the output area. The focus is given on the waveform and not on the magnitude. The waveform of $p_{ext}$ is derived from the two previous equations: in the time domain, it is proportional to the (delayed) time derivative of the quantity $q_1^+(t)$:

$$p_{ext}(t, r) \propto \frac{dq_1^+}{dt}\left(t - \frac{\ell + r}{c}\right). \quad (34)$$

Notice that the waveform of $p_{ext}$ does not depend on the area $S_2$. It is thus not necessary to define this latter in the model. Using Eqs. (18), $q_1^+$ is eliminated in favor of $p_1^+$ and $p_1$, and a finite difference approaches the derivative operation, so that the digital radiated pressure is computed as

$$p_n^{ext}(r) = \frac{x_1}{x_s}\left(p_{1n}^+ - p_{1\,n-1}^+\right) - \frac{p_{1n}}{2}, \quad (35)$$

where the propagation delay equal to $(\ell + r)/c$ is ignored.

In comparison to the simple monopole model for cylinder, the term $p_{1n}/2$ appears to be due to the spherical waves in the duct. Digital experiments are performed with this definition, and the removal/inclusion of this term does not change visibly the waveform of the radiated pressure. This is due to the main contribution of the higher frequencies, which can be observed in the complicated shape of the signal (see Fig. 4). Secondly, the convergence of the external pressure waveform when increasing the sampling frequency (or, equivalently, decreasing $x_s$) is slower than for the internal pressure. This appears to be related to the high-pass filtering of the monopole model. This filtering is limited by the finite sampling frequency and the finite difference approximation of the derivation, and higher sampling frequencies are required to preserve the high-frequency spectral content. Finally, concerning the convergence when the mouthpiece length tends to 0, it appears to be also slower than that for the internal pressure.

## V. TRUNCATED CONE WITH A LUMPED MOUTHPIECE (SECOND MODEL)

### A. Continuous-time model

The results of the previous model suggest another approach of the mouthpiece role: the mouthpiece can be considered as a simple compliance in parallel, $V_m/(\rho c^2)$, with $V_m = S_1 x_1/3$, as shown in Fig. 8. This means that the mouthpiece does not add any geometrical parameter to the two of the truncated cone. In the frequency domain, the equations for the mouthpiece are:

$$P = P_1 \text{ and } U = U_1 + j\omega\frac{V_m}{\rho c^2}P, \quad (36)$$

where $P$ and $U$ are the pressure and the flow rate at the mouthpiece input. They can be decomposed

in the variables $P^+ = (P + \rho cU/S_1)/2$ and $P^- = (P - \rho cU/S_1)/2$. Then, using Eqs. (11), $P_1$ and $U_1$ are eliminated:

$$P^+ + P^- = Q_1^+ + Q_1^-;$$
$$P^+ - P^- = Q_1^+ - Q_1^- + \frac{P}{jkx_1} + \frac{jkx_1P}{3}. \quad (37)$$

The spherical wave variables write down, in the time domain, to:

$$q_1^-(t) = p^-(t) + \frac{c}{2x_1}\int_0^t p(t')dt' + \frac{x_1}{6c}\frac{dp}{dt}(t), \quad (38)$$

$$q_1^+(t) = p^+(t) - \frac{c}{2x_1}\int_0^t p(t')dt' - \frac{x_1}{6c}\frac{dp}{dt}(t); \quad (39)$$

and the lossless propagation and reflection at the open end of the cone $q_1^-(t) = -q_1^+(t - \tau)$ gives

$$\frac{dp}{dt}(t) = \frac{dp}{dt}(t - \tau) - \frac{6c}{x_1}\left(p^-(t) + p^+(t - \tau)\right.$$
$$\left. + \frac{c}{2x_1}\int_{t-\tau}^t p(t')dt'\right). \quad (40)$$
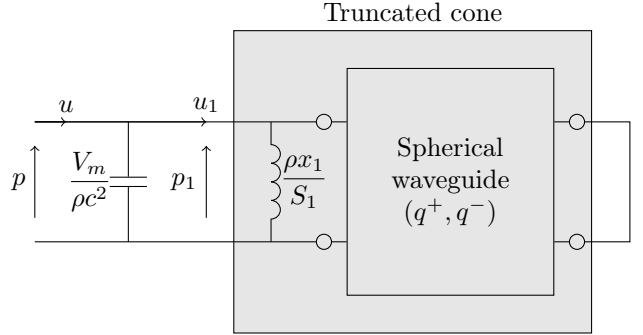


Figure 8: Equivalent circuit of the model with a lumped mouthpiece.

### B. Discretization

As in Sec. IV.C, the integral term $\frac{c}{2x_1}\int_{t-\tau}^t p(t')dt'$ in Eq. (40) is approached by $I_n$ using the trapezoidal rule:

$$I_n = I_{n-1} + \frac{x_s}{4x_1}\left(p_n + p_{n-1} - p_{n-2M} - p_{n-1-2M}\right). \quad (41)$$

In addition, the derivative terms are estimated by the finite differences:

$$\frac{dp}{dt}(t) \simeq \frac{p_{n+1} - p_n}{t_s}, \quad (42)$$

so that the following result is obtained:

$$p_{n+1} = p_n + p_{n-2M+1} - p_{n-2M}$$
$$- \frac{6x_s}{x_1}\left(p_n^- + p_{n-2M}^+ + I_n\right). \quad (43)$$

For the *ab-initio* calculation, the following quantities are evaluated sequentially at each time step: $I_n$

(Eq. (41)), $p_{n+1}$ (Eq. (43)), $u_{n+1}$ using the nonlinear characteristics $F$ (Eq. (3)) for the coupling with the excitation, and at last $p_{n+1}^{\pm}$.

The external sound is derived from Eqs. (34) and (39):

$$p_n^{ext} = \frac{x_1}{x_s} \left( p_n^+ - p_{n-1}^+ \right) - \frac{p_n}{2}$$
$$- \frac{1}{6} \left( \frac{x_1}{x_s} \right)^2 (p_{n+1} - 2p_n + p_{n-1}). \qquad (44)$$

### C. Discussion

This algorithm computes the minimum model of reed conical instruments, generalizing the iterated map algorithm for cylindrical instruments, with only one additional parameter, the distance to the apex $x_1$. The model considers only two parameters for the definition of the truncated cone, the lengths of the missing part, $x_1$ and of the truncated cone, $\ell$. This means that only the ratio of the input and output radii is fixed, and therefore the apex angle is not fixed.

Figs. 4 and 5 compare the results with those of the first model. The results of the two models are consistent when the length of the cylindrical mouthpiece $y$ is very short ($y \leq 10mm$) for all the quantities but the external pressure. This is intuitive: if the length $y$ becomes very short in comparison with the wavelength, the mouthpiece can be represented by two lumped elements: a fixed shunt acoustic compliance, $V_m/\rho c^2$, and an acoustic mass in series $M_m = \rho y/S_m = \rho y^2/V_m$ that tends to 0. Therefore the remaining effect when decreasing $y$ is due to the compliance only, which does not depend on the length $y$.

For the external pressure, a correct superposition of the waveforms is found after the compensation for the delay. However there are small differences from the result of the first model. Some peaks can be observed. Several expressions for the derivatives (of first and second order) involved in Eq. (40) have been empirically tested, and the expression chosen ensures the weakest peaks. The stability of this algorithm is studied in Appendix A.2.

A major interest of this second algorithm is the direct use of the nonlinear function $F$ (Eq. (1)). The problem can be solved without any kind of ambiguity that affect the rotated function $G$. It is a useful tool to study the effect of the nonlinear characteristic on the sound production. When several solutions exist with the first model (Sec. IV), i.e., when $\zeta > 1$, the second model allows understanding how the selection of the solution could be done (see Ref. 16). Figure 9 shows for the same geometry the influence of the reed opening $\zeta$: when $\zeta$ increases, the minimum value of the pressure diminishes, and the oscillations of the positive pressure increase. This corresponds to an enrichment of the spectrum. For very small values of $\zeta$, the waveform becomes very different from a Helmholtz motion. Notice that other algorithms can avoid the inversion or simplify to the solving of a quadratic equation, for instance, taking the reed dynamics into account.[14,33]
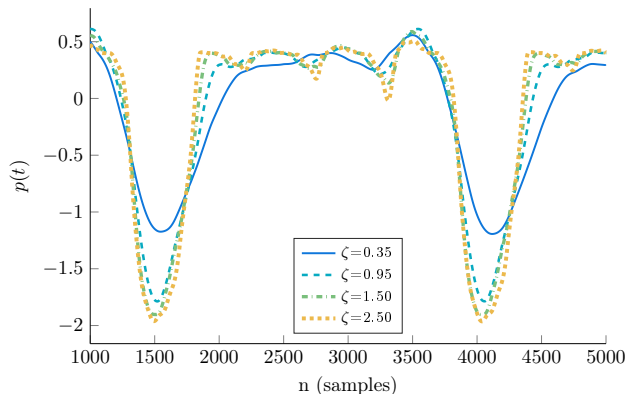


Figure 9: (Color online) Influence of the parameter $\zeta$ on the mouthpiece pressure $p(t)$ for the second model. Solid line: $\zeta = 0.35$. Dashed line: $\zeta = 0.95$. Dash-dotted line: $\zeta = 1.50$. Dotted line: $\zeta = 2.5$. The other parameters are the same as those of Fig. 4.

### D. An attempt of comparison with experiment

The measurement of the mouthpiece pressure of a baritone saxophone has been performed by B. Gazengel using the experimental device presented in Ref. 34. The ability of the second model to reproduce the waveform of the lowest note (C2, 65.4Hz) is tested here. The lack of the values for the excitation parameters $p_M$ and $S_{op}$ in the measurement prohibits a direct sample-based comparison. Instead a Fourier analysis of the steady part of the measured signal is used to estimate the oscillation frequency $f_{osc}^{meas}$ and the coefficients $C_k^{meas}$ of the Fourier series. These latter are normalized with respect to the fundamental coefficient and the DC component ($k = 0$) is ignored as the static component has not been measured by the microphone. $f_{osc}^{mod}$ and $C_k^{mod}$ can be similarly obtained by simulation using the second model. An nonlinear least-squares optimization then seeks for the values of the parameters $\ell + x_1$, $x_1$, $\gamma$ and $\zeta$ of the second model that minimize the compound function cost $\mathcal{F}$:

$$\mathcal{F}(\ell + x_1, x_1, \gamma, \zeta) = \left( 1 - \frac{f_{osc}^{mod}(\ell + x_1, x_1, \gamma, \zeta)}{f_{osc}^{meas}} \right)^2$$
$$+ \alpha \sum_{k=1}^{10} \left| C_k^{mod}(\ell + x_1, x_1, \gamma, \zeta) - C_k^{meas} \right|^2. \quad (45)$$

The weighting parameter $\alpha$ is set so as to balance the relative error on the oscillation frequency, and the error on the first ten coefficients $C_k$ of the Fourier series (i.e the r.m.s. value of the difference of the synchronized signals, due to the Parseval's identity). The cost function appears to be a globally smooth function of the parameters but with some deep narrow valleys, so that the results shown on Fig. 1 (obtained for $\alpha = 4 \times 10^{-4}$) may only correspond to a local optimum.

Nevertheless, the triangle-shaped negative episode and the oscillation increase in the positive episode indicate that the presented model is able to reproduce the features of the measured signal, which is not the case for the results of the cylindrical saxophone model

9

(also shown in Fig. 1, for the same values of parameters $\gamma$, $\ell$ and $x_1$). The excitation parameters are found to be plausible, as well as the geometrical ones: the latter could be obtained by measurements, but this would require the use of accurate models for closed toneholes, changes in taper, bends, radiation, etc.

### E. Regularized nonlinear characteristic

It is interesting to look at a more "realistic" model, avoiding the two discontinuities in the nonlinear characteristic. The second model allows doing the computation easily. As discussed in Sec. II, Eq. (3) exhibits two singularities. The regularization (i.e. the increase of derivability) of the first one, $\left[1 - \gamma + \frac{p}{p_M}\right]^+$, makes sense considering the results in Ref. 3 (Fig. 3) which shows that the flow smoothly vanishes when the mouth pressure exceeds the "beating reed pressure". The following regularization is suggested:

$$[x]^+ \to H_1(x) = \frac{1}{\pi} + \frac{x}{O_a}\left(\frac{1}{2} + \frac{\arctan(x/O_a)}{\pi}\right),$$
(46)

that is tunable by means of the parameter $O_a$ (here set to 0.1) and ensures that the flow remains a non-negative monotonic $C_\infty$ function of the aperture $1 - \gamma + \frac{p}{p_M}$.

The singularity of the flow at the vanishing pressure difference corresponds to the term $\mathrm{sign}\,(\Delta p)\sqrt{|\Delta p|}$, i.e., the change in sign of the acoustic flow. The flow derivative becomes singular and therefore no sampling would theoretically be possible without aliasing. Nevertheless, the second regularization

$$\mathrm{sign}\,(x)\sqrt{|x|} \longrightarrow H_2(x) = \mathrm{sign}\,(x)\sqrt{x}\,\tanh(x/V_a),$$
(47)

(with default value 0.05 for the parameter $V_a$) guarantees a bounded flow derivative. Finally, a smoothed nonlinear characteristic writes down to:

$$F(p) = \zeta p_M H_1\left(1 - \gamma + \frac{p}{p_M}\right)H_2\left(\gamma - \frac{p}{p_M}\right).$$
(48)

The non-regularized model given in Eq. (3) can be recovered by giving very small values to $O_a$ and $V_a$ (typically $10^{-10}$). As shown in Fig. 10, the effect is not negligible, but a zoom is useful in order to exhibit it. The abrupt angles in the flow rate signal disappear, due to the first regularization. The effect of the regularization near zero flow appears in the negative part of the flow rate curve. Concerning the external pressure, the regularization suppresses small peaks in the signal, and allows the amplitude to diminish at higher frequencies.
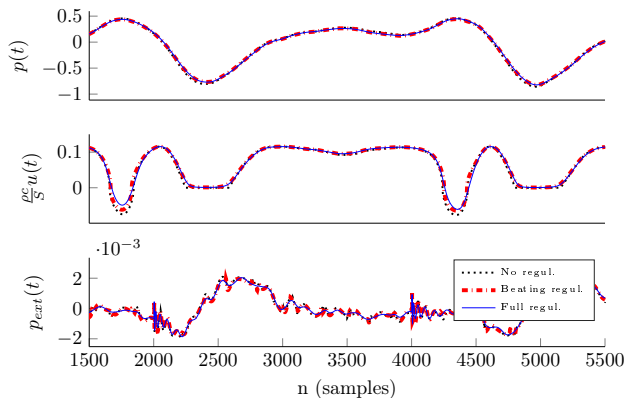


Figure 10: (Color online) Effect of the regularization on the signal shapes for the second model. The parameters are those of Fig. 4. Thin solid line: result for the two regularizations. Thick dashed line: result for the regularization at the beating limit. Thin dotted line: result without regularization.

## VI. CONCLUSION, FURTHER WORK

The waveforms found using the two models which have been investigated are similar to measured ones for various conical instruments, with the condition, for the first model, that the length of the cylindrical mouthpiece is not too long ($\mu > 1.5$). The second model gives the same results as the first one for small lengths, with small differences in the radiated sound. This was not obvious, because the algorithms are rather different. It appears that the main characteristic of the waveform produced by conical reed instruments depends neither on the reed dynamics nor on the losses. These characteristics only rely on the two geometrical parameters of the second model, i.e., $x_1$ and $\ell$. In this model, the geometry is not fully defined, as the value of the apex angle (and thus the input and output radii of the truncated cone) need not to be defined. It would only get involved when accounting for losses in the bore. This means that the apex angle is a parameter of minor importance in comparison with the length of the missing cone.

The second model can be used for a more systematic study with respect to the excitation and geometrical parameters: obviously one limit of the existence of this kind of waveform is that the ratio $x_1/\ell$ remains small enough, because if this ratio tends to infinity, the resonator tends to a cylinder, with a different waveform. Studies of the different regimes with bifurcation schemes or regime maps can be done in a way generalizing previous works on cylindrical resonators. This can be easily done, with a possibility to modify the nonlinear characteristic. The sampling frequency can be very large, in particular for higher instruments (requiring small sampling length), but this drawback is not crucial for the above purpose.

The first model fills the gap between the model with a lumped mouthpiece and the "cyclone" model.[28,29]. By allowing the cross-section area of the cylindrical

mouthpiece to vary, it can be used to study the role of the resonance inharmonicity on the functioning: indeed By tuning the length $y$ of the mouthpiece (see Fig. 7), it is possible to go continuously from a positive to a negative inharmonicity.

### Acknowledgements

## A. STABILITY ANALYSIS OF THE TWO ALGORITHMS

The implementations of the two models are analyzed in order to study the stability of the digital schemes, using the $z$-transform framework (see, e.g., Ref. 35).

### A.1. Model with cylindrical mouthpiece

From Eqs. (25)-(26), it is straightforward to check that the continuous-time formulation is associated in the frequency domain to the reflection coefficient:

$$R(\omega) = \frac{P^-(\omega)}{P^+(\omega)} = e^{-2jky}\frac{\mu - \mathcal{Y}_{cone}(\omega)}{\mu + \mathcal{Y}_{cone}(\omega)} \quad (49)$$

$$\text{with } \mathcal{Y}_{cone}(\omega) = \frac{1}{j\tan(k\ell)} + \frac{1}{jkx_1}. \quad (50)$$

$\mathcal{Y}_{cone}(\omega)$ is the dimensionless input admittance of the truncated cone. Taking the z-transform of Eqs. (29), (30) and (31), the discrete-time transfer function is obtained replacing $\mathcal{Y}_{cone}$ by its discrete counterpart:

$$\mathcal{Y}_d(z) = \frac{1 + z^{-2M}}{1 - z^{-2M}} + \frac{x_s}{2x_1}\frac{1 + z^{-1}}{1 - z^{-1}}. \quad (51)$$

Restraining to the unit circle $z = e^{\frac{j\omega}{f_s}}$ ($f_s$ is the sampling frequency),

$$\mathcal{Y}_d(z = e^{\frac{j\omega}{f_s}}) = \frac{1}{j\tan\frac{M\omega}{f_s}} + \frac{1}{j\frac{2x_1}{x_s}\tan\frac{\omega}{2f_s}} \quad (52)$$

directly relates to Eq. (50) considering a low-frequency approximation of the last term. The digital reflection coefficient is guaranteed to have a modulus equal to 1, as the admittance $\mathcal{Y}_s$ is purely imaginary. Thus the proposed algorithm provides a stable implementation of the first model.

### A.2. Model with lumped mouthpiece

Eq. (37) gives the dimensionless input admittance of the truncated cone with a lumped mouthpiece:

$$\mathcal{Y}'(\omega) = \frac{U(\omega)}{P(\omega)} = \frac{1}{j\tan(k\ell)} + \frac{1}{jkx_1} + \frac{jkx_1}{3}. \quad (53)$$

Denoting $\mathbb{D}(z)$ and $\mathbb{I}(z)$ the $z$-transform of the digital implementation of the derivation and integration,[35] the discrete transfer function is

$$\mathcal{Y}'_d(z) = \frac{1 + z^{-2M}}{1 - z^{-2M}} + \frac{c}{x_1}\mathbb{I}(z) + \frac{x_1}{3c}\mathbb{D}(z). \quad (54)$$

The passivity of this model is given by the sign of the real part of the input admittance on the unit circle $z = e^{j\omega/f_s}$:

$$\text{Re}\left(\mathcal{Y}'_d(e^{\frac{j\omega}{f_s}})\right) = \frac{c}{x_1}\text{Re}\left(\mathbb{I}(e^{\frac{j\omega}{f_s}})\right) + \frac{x_1}{3c}\text{Re}\left(\mathbb{D}(e^{\frac{j\omega}{f_s}})\right), \quad (55)$$

which has to be positive.

Several choices are possible for the operators $\mathbb{D}(z)$ and $\mathbb{I}(z)$. While implicit methods (right rectangle integration rule and/or implicit Euler derivation) tend to be stabilizing (leading to a positive real part of the admittance), explicit ones are destabilizing (left rectangle integration rule and/or explicit Euler derivation) and zero-phase operators (trapezoidal integration and bilinear or centered derivation) are neutral. The combinations induce stability properties (stable/unstable) that may be unconditional (on the whole frequency range) or not. The choice made in Sec. V with an explicit Euler derivation and a trapezoidal rule integration

$$\mathbb{D}(z) = f_s\frac{1 - z^{-1}}{z^{-1}} \quad \text{and} \quad \mathbb{I}(z) = \frac{1}{2f_s}\frac{1 + z^{-1}}{1 - z^{-1}} \quad (56)$$

is known to produce an unstable acoustic resonator whose impulse response has a slowly increasing non-causal component. However this still allows the simulation of self-sustained oscillations when coupling with the excitation, without supplementary features such as for example reed dynamics. The oscillation thresholds may be altered but this is beyond the scope of the present paper. It is also worth noticing that impulse responses obtained with conservative approximations of the lumped elements may also suffer from digital instabilities due to the non–vanishing of the reflection coefficient at the Nyquist frequency.

### References

1. M. E. McIntyre, R. T. Schumacher, and J. Woodhouse, "On the oscillations of musical instruments", J. Acoust. Soc. Am. 74,1325–1345 (1983).

2. T. Wilson and G. Beavers, "Operating modes of the clarinet", J. Acoust. Soc. Am. 56, 653–658 (1974).

3. J.-P. Dalmont, J. Gilbert, J. Kergomard, and S. Ollivier, "An analytical prediction of the oscillation and extinction thresholds of a clarinet", J. Acoust. Soc. Am. 118, 3294–3305 (2005).

4. P.-A. Taillard, J. Kergomard, and F. Laloë, "Iterated maps for clarinet-like systems", Nonlinear dynamics 62, 253–271 (2010).

5. P.-A. Taillard and J. Kergomard, "An analytical prediction of the bifurcation scheme of a clarinet-like instrument: Effects of resonator losses", Acta Acust. united Ac. 101, 279–291 (2015).

6. J.-P. Dalmont, C. Frappé, "Oscillation and extinction thresholds of the clarinet: Comparison of analytical results and experiments". J. Acoust. Soc. Am. 122 1173–1179 (2007).

7. A. H. Benade and S. J. Lutgen, "The saxophone spectrum", J. Acoust. Soc. Am. 83, 1988, 1900-1907.

8. J.-P. Dalmont, J. Gilbert, and J. Kergomard, "Reed Instruments, from small to large amplitude periodic oscillations and the Helmholtz motion analogy", Acta Acust. united Ac. 86, 671-684 (2000).

9. A.H. Benade, "Equivalent circuits for conical waveguides", J. Acoust. Soc. Am. 83, 1764-1769 (1988).

10. S. Ollivier, J.-P. Dalmont, and J. Kergomard, "Idealized Models of Reed Woodwinds. Part I: Analogy with the Bowed String", Acta Acust. united Ac. 90, 1192-1203 (2004).

11. A. Ya. Gokhshtein, "Pressure jumps in the reflection of a wave from the end of a tube and their effect on the pitch of sound", Sov. Phys. Doklady 25, 462-464 (1980).

12. M. Shimizu, T. Naoi, and T. Idogawa, "Vibrations of the reed and the air column in the bassoon", J. Acoust. Soc. Jpn. 10, 269-278 (1989).

13. S. Carral and V. Chatziioannou, "Influence of the truncation length of the oboe cone on the reed closing time", Proc. 3rd Vienna Talk on Music Acoustics, Univ. Music & Perf. Arts Vienna (2015).

14. Ph. Guillemain, J. Kergomard, and Th. Voinier, "Real-time synthesis of clarinet-like instruments using digital impedance models", J. Acoust. Soc. Am. 118, 483-494 (2005).

15. J. B. Doc, Ch. Vergez and S. Missoum, "A Minimal Model of a Single-Reed Instrument Producing Quasi-Periodic Sounds", Acta Acust. united Ac. 100, 543-554 (2014).

16. J. Kergomard, Ph. Guillemain, and F. Silva, "Choice of algorithms for reed instruments oscillations: how to solve the equation for the nonlinear characteristics?", Proc. Acoustics, 1161-1166, Nantes 2012.

17. A. M. Hirschberg, "Aero-Acoustics of Wind Instruments", in "Mechanics of Musical Instruments" edited by A. Hirschberg, J. Kergomard, and G. Weinreich (CISM Courses and Lectures, Springer, Wien, 1995), vol. 335, 291–369.

18. A. Almeida, Ch. Vergez, and R. Caussé, "Quasi-static non-linear characteristics of double-reed instruments", J. Acoust. Soc. Am. 121, 536-546 (2007).

19. J. C. Schelleng, "The bowed string and the player", J. Acoust. Soc. Am. 53, 26–41 (1973).

20. C. Maganza, R. Caussé, and F. Laloë, "Bifurcations, period doubling and chaos in clarinetlike systems", Europhysics letters 1, 295–302 (1986).

21. A. H. Benade and W. Bruce Richards, "Oboe normal mode adjustment via reed and staple proportioning", J. Acoust. Soc. Am. 73, 1794-1803 (1983).

22. J. Kergomard, A. Lefebvre and G.P. Scavone, "Matching of Fundamental Modes at a Junction of a Cylinder and a Truncated Cone; Application to the Calculation of Some Radiation Impedances", Acta Acust. united Ac. 101, 1189-1198 (2015).

23. J. Agulló, A. Barjau, J. Martinez, "Alternatives to the impulse response h(t) to describe the acoustical behavior of conical ducts", J. Acoust. Soc. Am. 84, 1606-1612 (1988).

24. J. Martinez and J. Agulló, "Conical bores, Part I: Reflection functions associated with discontinuities", J. Acoust. Soc. Am. 84, 1613-1619 (1988).

25. J. Gilbert, J. Kergomard, and J. D. Polack, "On the reflection functions associated with discontinuities in conical bores", J. Acoust. Soc. Am. 7, 1773-1780 (1990).

26. A. Almeida, Physical models of double reeds applied to sound synthesis (Ph.D. dissertation, Univ. Pierre & Marie Curie, Paris, 2006).

27. J.-P. Dalmont, B. Gazengel, J. Gilbert, and J. Kergomard, "Some Aspects of Tuning and Clean Intonation in Reed Instruments", Applied Acoustics 46, 19-60 (1995).

28. M. van Walstijn and M. Campbell, "Discrete-time modeling of woodwind instrument bores using wave variables", J. Acoust. Soc. Am. 113, 575–585 (2003).

29. G. Scavone, "Time-domain synthesis of conical bore instrument sounds", Proc. Int. Comp. Music Conf., Göteborg, 9-15 (2002).

30. A. Hirschberg and J. Kergomard, "Introduction", in "Mechanics of Musical Instruments" edited by A. Hirschberg, J. Kergomard, and G. Weinreich (CISM Courses and Lectures, Springer, Wien, 1995), vol. 335, 3.

31. J.-B.Doc and Ch. Vergez, "Oscillation regimes produced by an alto saxophone: Influence of the control parameters and the bore inharmonicity", J. Acoust. Soc. Am. 137, 1756-1765 (2014).

32. Th. Hélie and X. Rodet, "Radiation of a Pulsating Portion of a Sphere: Application to Horn Radiation", Acta Acust. united Ac. 89, 565–577 (2003).

33. Ph. Guillemain, "A digital synthesis model of double-reed wind instruments", J. Appl. Sig. Proc. 7, 990-1000 (2004).

**34.** B. Gazengel and J. P. Dalmont, "Mechanical response characterization of saxophone reeds", Forum Acusticum, Aalborg (2011).

**35.** J.O. Smith, "The Z Transform", in Introduction to Digital Filters with Audio Applications, W3K Publishing, 2007.

**Figure Captions**

Fig. 1 (Color online) Comparison of the measured mouthpiece pressure for a baritone saxophone on the lowest note C2 (65.4Hz, dash-dotted line) with the signal obtained using the second model presented in the current paper (using $\ell = 2.272m$, $x_1 = 30.8cm$, $\gamma = 0.34$ and $\zeta = 0.51$, notations defined in Sec. IV, solid line) and with the rectangle signal obtained using the "cylindrical saxophone" model (same values of $\ell$, $x_1$ and $\gamma$, see Ref. 10, dotted line). The numerical result is discussed in Section V.D. Measurement done by B. Gazengel

Fig. 2 (Color online) Nonlinear characteristic $F(p)$. Solid line: $\zeta = 2.55$. Dotted line: $\zeta = 0.95$. The point A indicates the beating limit; the point B indicates the limit of negative flow rate. Between the dash-dotted lines, Eq. (8) has 3 solutions when $\zeta > 1$ (see Sec. III)

Fig. 3 Geometry and equivalent circuit of the model with a cylindrical mouthpiece. The geometry of the truncated cone is described by 2 parameters only: $x_1$ and $\ell$

Fig. 4 (Color online) Steady-state signals, for a very short length $y = 1mm$. From top to bottom: the dimensionless mouthpiece pressure $p(t)/p_M$; the flow rate at the input of the mouthpiece $u(t)$ times $\rho c/(S_1 p_M)$; the outgoing spherical wave $q_1^+(t)$ (arbitrary scale); the external pressure $p_{ext}(t)$ (arbitrary scale). The geometrical parameters are similar to those of a baritone saxophone ($\ell = 1m$, $x_1 = 0.3m$), the non dimensional mouth pressure and reed opening parameters are $\gamma = 0.4$, $\zeta = 0.95$, and the sampling length is $x_s = 1mm$. The dashed lines represent the result of the second model (see Section V)

Fig. 5 (Color online) Steady-state mouthpiece pressure $p(t)$ for various mouthpiece lengths $y$ (the parameter values are the same as those of Fig. 4). In abscissa, the number of samples. From top to bottom, the solid lines represent: $y = 1mm$ ($N = 1$, $\mu = 100$); $y = 10mm$ ($N = 10$, $\mu = 10$); $y = 70mm$ ($N = 70$, $\mu = 1.43$, value close to that of a real baritone saxophone); and $y = 100mm$ ($N = 100$, $\mu = 1$). For all plots the dashed line is the same: it represents the result of the second model

Fig. 6 (Color online) Fundamental frequency (upper axes) and magnitude of the Fourier coefficients (lower axes) of the steady-state pressure signal as functions of the mouthpiece length $y$. The corresponding cross-section ratios values $\mu$ are also reported on the top of the upper axes. $C_1$ relates to the fundamental tone and $C_{n \geq 2}$ to the higher harmonics. All the other parameters values are the same as in Fig. 4

Fig. 7 (Color online) Inharmonicity relative to the first resonance frequency of the first model, with respect to the mouthpiece length $y$ (all other parameters values are the same as Fig. 4)

Fig. 8 Equivalent circuit of the model with a lumped mouthpiece

Fig. 9 (Color online) Influence of the parameter $\zeta$ on the mouthpiece pressure $p(t)$ for the second model. Solid line: $\zeta = 0.35$. Dashed line: $\zeta = 0.95$. Dash-dotted line: $\zeta = 1.50$. Dotted line: $\zeta = 2.5$. The other parameters are the same as those of Fig. 4

Fig. 10 (Color online) Effect of the regularization on the signal shapes for the second model. The parameters are those of Fig. 4. Thin solid line: result for the two regularizations. Thick dashed line: result for the regularization at the beating limit. Thin dotted line: result without regularization